Instruments of RT-2 Experiment onboard CORONAS-PHOTON and their test and evaluation III: Coded Aperture Mask and Fresnel Zone Plates in RT-2/CZT Payload

Anuj Nandi · S. Palit · D. Debnath · Sandip K. Chakrabarti · T. B. Kotoch · R. Sarkar · Vipin K. Yadav · V. Girish · A. R. Rao · D. Bhattacharya

Abstract Imaging in hard X-rays of any astrophysical source with high angular resolution is a challenging job. Shadow-casting technique is one of the most viable options for imaging in hard X-rays. We have used two different types of shadow-casters, namely, Coded Aperture Mask (CAM) and Fresnel Zone Plate (FZP) pair and two types of pixellated solid-state detectors, namely, CZT and CMOS in RT-2/CZT payload, the hard X-ray imaging instrument onboard the CORONAS-PHOTON satellite. In this paper, we present the results of simulations with different combinations of coders (CAM

A. Nandi[+], S. Palit, D. Debnath, T. B. Kotoch, R. Sarkar and Vipin K. Yadav[+]
Indian Centre for Space Physics, 43 Chalantika, Garia Station Road, Kolkata 700084
Tel.: +91-33-24366003
Fax: +91-33-24622153 Ext. 28
E-mail: anuj@csp.res.in; sourav@csp.res.in; dipak@csp.res.in; tilak@csp.res.in; ritabrata@csp.res.in; vipin@csp.res.in (+: Posted at ICSP by Space Science Division, ISRO Head Quarters)

Sandip K. Chakrabarti
S.N. Bose National Centre for Basic Sciences, JD Block, Salt Lake, Kolkata 700097
(Also at Indian Centre for Space Physics, 43 Chalantika, Garia Station Rd., Kolkata 700084)
Tel.: +91-33-23355706
Fax: +91-33-23353477
E-mail: chakraba@bose.res.in

V. Girish
Space Astronomy and Instrumentation Division, ISAC, Bangalore, 560017
E-mail: giri@isac.gov.in

A. R. Rao
Tata Institute of Fundamental Research, Homi Bhabha Road, Colaba, Mumbai, 400005
E-mail: arrao@tifr.res.in

D. Bhattacharya
Inter-University Centre for Astronomy and Astrophysics, Ganeshkhind, Pune, 411007
E-mail: dipankar@iucaa.ernet.in

& FZP) and detectors that are employed in the RT-2/CZT payload. We discuss the possibility of detecting transient Solar flares with good angular resolution for various combinations. Simulated results are compared with laboratory experiments to verify the consistency of the designed configuration.

Keywords Zone plates · X- and gamma-ray telescopes and instrumentation · Fourier optics · X-ray imaging

PACS 42.79.Ci · 95.55.Ka · 42.30.Kq · 87.59.-e

1 Introduction

Imaging astrophysical sources in X-rays of electro-magnetic wave band, specially in hard X-rays, is really a challenging and difficult task. X-ray photons do not efficiently get reflected or refracted because of their ability to penetrate deep into the interacting material. It is, however, possible to image with soft X-ray photons by making them hit a highly polished mirror at a small angle to the reflecting surface. This process, called grazing incidence imaging technique, is effective mainly for soft X-rays (up to ~ 10 keV). For example, in *Chandra* and *XMM-Newton* missions, soft X-ray imaging has been done very successfully with this technique. Unfortunately, this direct imaging technique is very difficult to implement for hard X-rays and γ-rays.

Instead of direct imaging, some indirect imaging techniques have been developed and adopted for imaging in hard X-rays as well as in γ-rays. Shadow casting method is one such efficient indirect imaging technique (Mertz & Young 1961). This technique is based on the total absorption of hard X-rays by the shadow-caster, allowing the generation of patterns in the detector plane, which can be deconvolved to get the source image. There are various types of shadow casting methods depending on the structure of coder and mask pattern. One such approach is to use a single plane coder, namely Coded Aperture Mask (CAM), which is widely used in different astronomical observations (Dicke 1968, Ables 1968, Baker et al., 1983 and Caroli et al., 1987). In this approach, mask pattern is basically followed by the individual pixel dimension of the detector and therefore, the angular resolution depends on the separation between the coder and the detector plane and the smallest size of the coder element.

Another approach (Mertz & Young 1961, Desai et al., 1998, Chakrabarti et al., 2009) to image in hard X-rays with high angular resolution is to use double plane coder of Fresnel Zone Plates (FZPs). The high angular resolution, which is achievable upto a few arc-sec through this method depends on the outermost zone width and separation between the two coders (pair of FZP) (Palit et al., 2009).

RT-2/CZT payload, one of the most important instruments of the RT-2 experiment (Debnath et al. 2009, Kotoch et al. 2009, Sarkar et al. 2009, Sreekumar et al. 2009) onboard CORONAS-PHOTON mission (Kotov et al. 2008, Nandi et al. 2009), is specially designed to provide high resolution spectral and imaging information of hard X-ray solar flares at energies above 20 keV. For this, we have employed both the shadow casting methods - the Coded aperture mask (CAM) and dual Fresnel zone plate (FZP) as a coder in RT-2/CZT payload. Detection of hard X-rays requires interaction of photons with denser and heavy material and for imaging, position sensitivity is also essential for the detector. We have used two types of solid-state pixellated detectors, namely, Cadmium Zinc Telluride (CZT) and Complementary Metal Oxide Semiconductor (CMOS) detectors in RT-2/CZT payload. The solid-state CZT detector has a

very good combination of energy resolution, detection efficiency and it is best suited with CAM pattern in terms of required spatial resolution. On the other hand, the CMOS detector, with high positional accuracy, is very good for imaging purposes and with the combination of FZP it can give a few arc-sec of angular resolution.

X-ray observation of solar flares must be made from a platform launched above the atmosphere. Sending such instrument to near space by balloon is an option. But the best way is to send it through a satellite orbiting the Earth. Many missions, like *GRANAT*, *HETE*, *SWIFT* etc. had included shadow casting method for imaging in hard X-rays.

All of these mission employ CAM and they are for imaging mainly of celestial objects like AGNs, compact objects and GRBs. RT-2 will be the first of its kind to use both types of shadow caster (CAM & FZP) for studying hard X-ray solar flares.

In this paper, we discuss in detail the coders and detectors employed in the RT-2/CZT payload. We also provide simulation results along with some laboratory test results to validate these simulations. In the next section, we discuss the principle of operation of CAM and FZP as shadow casters and their basic constructions. This includes the theory behind the working principle and the image reconstruction processes. In the same section the specifications of the instruments, viz, detectors and shadow casters are given. Then in section 3, we discuss the angular resolution (AR) and field of view (FOV) of all four combinations of coder and detector used in the payload and make comparative study of them in terms of these two important characteristics. In section 4, we present the simulation aspects of each configuration used in this payload. These include shadow formations (eg. Moiré fringe for FZPs) and source reconstruction for one or more sources. In section 5, we discuss what we expect in context of solar observation from the instrument used in this experiment. The results of the laboratory experiments carried out with the designed instruments are presented in section 6. Finally, in section 7, we make some concluding remarks.

2 CAM and FZP as shadow masks

Coded mask imaging is a class of spatial multiplexing technique (Caroli et al., 1987) for imaging of objects in high energy part of the electromagnetic spectrum, specially in X-rays & γ-rays. It is a two step process in which data is acquired from some part of the sky (within FOV of the instrument) and source image is reconstructed by some computation procedures. A coded mask is a plate consisting of areas which are transparent and opaque to photons within certain energy ranges. The transparent and opaque areas or mask elements are generally of equal size and are distributed in a predetermined pattern. The mask acts as a shadow caster, viz, shadows of the mask are projected on the detector placed below the mask facing the sky, by the rays coming from the sources in the visible part of the sky. The projected shadow on the detector plane has the same coding information as that of the mask pattern. The information on the directions of the rays falling on the mask and hence the source positions in the field of view are encoded in the amounts of shift of all the shadow patterns with respect to the central position and the information on the source intensities are encoded in the strengths of the patterns.

2.1 Coded Aperture Mask (CAM)

2.1.1 CAM as a coder

A pinhole camera has the characteristics required for a proper indirect imaging performance, but it has poor signal-to-noise ratio. The sensitivity (signal to noise - S/N - ratio) may be increased by increasing the pinhole area but at the same time it will degrade the angular resolution of the device. A random pinhole camera (Dicke 1968 and Ables 1968) can be constructed by placing many pinholes at random in a plate. This increases the open area of the plate, required for better sensitivity and also preserves the angular resolution. It is found that ideal patterns for random pinhole camera should be based on cyclic difference sets (Gunson & Polychronopulos 1976, Fenimore & Cannon 1978). It is also required that every detector pixel is exposed to one full mask pattern. These patterns are also called Uniformly redundant arrays (URA) (Fenimore & Cannon 1978).

In RT-2/CZT, CZT detector modules of 256 pixels of size $\sim 2.5 \times 2.5$ mm^2 are used (see Kotoch et al. 2009 for details). For good hard X-ray spectroscopic observations, it is necessary to have individual pixel calibration and simultaneous background measurements. Hence, the individual pixel reading capability of these modules can be effectively used by incorporating an appropriate coder for the purpose of simultaneous background measurement. Further, solar hard X-ray emission (above 20 keV) is observable only during hard X-ray flares which generally are associated with some active regions. Hence an identification of the active region on the solar surface during solar hard X-ray flares, correct to arc-minute accuracy, would also be a desirable characteristics of the coder. A pseudo noise Hadamard set which is capable of giving maximum possible transmission (50 %) (Caroli et al., 1987, In't Zand 1992) is suitable for a mask employing CZT detector module. For the detector of 256 pixels, we chose 256 mask elements (to maximize the localization accuracy). Since a pseudo noise Hadamard set has 2^m-1 elements, we chose m = 8 with an extra opaque element in the mask.

A pseudo noise Hadamard set is constructed from a shift-register algorithm (Peterson 1961). The coefficients p_j of a mth order primitive polynomial (all the coefficients are either 1 or 0) can be used as the generating function of a mask pattern of length 2^m-1, provided the polynomial is also an irreducible one. The mask elements a_i where i = 0, 2^m-2 can be generated from the coefficients by using the shift register algorithm

$$a_{i+m} = \sum_{j=0}^{m-1} p_j \times a_{i+j} (mod \ 2).\qquad(1)$$

The above mentioned process for m = 8 gives 16 polynomials from which CAM patterns may be generated. Out of these 16 options, the following two polynomials were chosen for the CZT-CAM configurations:

$$x^8 + x^6 + x^5 + x^2 + 1$$

and

$$x^8 + x^4 + x^3 + x^2 + 1.$$

The choice was made keeping in mind that each individual pixel should get possible maximum amount of mechanical support. These were determined by minimizing the

mechanical support parameter (MSP) defined as,

$$MSP = b + 4c + 8d,$$

where b corresponds to the number of segments of each pattern held at two or more corners, c and d corresponds to the number held respectively at 'one' and 'no' corner. The 'one' and 'no' corner elements have to be mechanically held to the neighboring closed elements, slightly reducing the open element area and hence reducing the sensitivity. The two patterns generated by the above two polynomials have the minimum MSP. For the 1st one

$$b = 3, \ c = 2, \ d = 0,$$

and for the 2nd one

$$b = 7, \ c = 1, \ d = 0.$$

And each of which gives MSP = 11. The two CAM patterns that are used in this payload are shown in Figure 4(a) and Figure 6(a).

2.1.2 Image reconstruction

The transformation from object distribution function in the sky, S(x,y) to the spatial distribution of the flux in the detector plane, D(x,y) can be mathematically written as (Caroli et al., 1987),

$$D(x,y) = C(x,y) * S(x,y) + B(x,y), \tag{2}$$

where $C(x,y)$ is the aperture transmission function, $B(x,y)$ is signal independent noise term and $*$ is the convolution operator. An estimation of the sky function ($S'(x,y)$) can then be made by filtering the detector flux distribution by a suitable decoding function $K(x,y)$ such that $K(x,y) * C(x,y)$ is a delta function. Therefore, the sky function can be written as,

$$S'(x,y) = K(x,y) * C(x,y) * S(x,y) + K(x,y) * B(x,y), \tag{3}$$

which is the reconstructed source distribution in the detector plane.

There are different types of reconstruction codes for CAMs, out of which suitable ones are chosen fulfilling the requirements of source informations. In our reconstruction process, all the above mentioned functions are represented as matrices. S is taken as a column matrix with number of elements equal to the total number of division i.e how the observed part of the sky is divided, and the value of each element is the source strength of corresponding divisions of the sky. D is the row matrix with number of elements equal to the number of detector pixels and each element representing the counts obtained in the corresponding pixels. Then C is defined as a matrix (a similar approach is followed by Caroli et al. 1987) whose number of column is equal to the number of elements in S and number of rows is equal to the number of elements of D, and C(i,j) is equal to 1 or 0 if the line joining the sky pixel corresponding to the j-th element of S and detector pixel corresponding to i-th element of D passes respectively through a transparent and opaque region of the CAM. Thus Eqn. 2 can be written as,

$$D = C * S + B,$$

where, B is a matrix which carries the noise information of the detector. Similarly, the sky function can be written in the matrix representation as,

$$S' = K * C * S + K * B,$$

Here, we use K as the matrix inverse to the matrix C. The operator $*$ simply denotes the matrix product. The distribution S' with some filtering by point spread function (PSF) gives near exact reconstruction of the object distribution. Object or source planes reconstructed by the above mentioned method from detector flux distributions, is verified with simulations and experimental results for various source distributions that are presented in §4 and §6 respectively. This method is used in this paper to get an idea of the source localization ability. For a good estimate of the source intensity, however, we plan to use a shadow fitting procedure, which can be fine-tuned to include experimental systematics like unequal pixel dimensions etc. (Ajello et al., 2008).

2.2 Fresnel Zone Plate (FZP) pair

2.2.1 Dual FZP as a coder

A Fresnel Zone Plate (FZP) coder is a dual plate coder, where two zone plates are placed at some distance apart. Fresnel zone plate has the following transmittance function (Barrett & Myers 2004, Chakrabarti et al., 2009)

$$T(r) = 1 \pm sgn[sin(\alpha r^2)]S(r), \tag{4}$$

where α is a parameter of the zone plate. S(r) is a support function (equals to 1 within the outer boundary of the zone plate and zero outside). The *sgn* function is +1 when $sin(\alpha r^2) > 0$ and - 1 when $sin(\alpha r^2) < 0$. Then the transmission function of the combined zone plates resembles a part of Fourier Transform (Mertz 1965) from source plane to detector plane. Zone plates are constructed such that α is related with n^{th} zone radius r_n by any one of the following equations,

$$\alpha r_n^2 = n\pi, \tag{5}$$

or

$$\alpha r_n^2 = (n \pm \frac{1}{2})\pi. \tag{6}$$

Taking two zone plates each of which with α satisfying either Eqn. 5 or Eqn. 6 and with + or - sign in Eqn. 6 (positive and negative zone plate), we can produce transmission function resembling any of the four parts of Fourier transform from source plane to detector plane (Chakrabarti et al., 2009).

One of the pair used in this payload (CONFIG-3) is a positive cosine pair, which implies that the shadow pattern produced in the detector is the positive cosine part of the Fourier transform (Chakrabarti et al., 2009). In this case, the radii of the nth zone of both the zone plates are given by

$$r_n = \sqrt{(n)}r_1, \tag{7}$$

where r_1 is the innermost zone radius and the central zones of the two zone plates are transparent.

The other pair (used in CONFIG-4) is a negative cosine pair. For this pair, the radius of the nth zone of both the zone plates are given by the same equation as that of the previous one but both the zone plates are negative in nature, i.e, the innermost zones are opaque to X-rays.

X-rays passing through two zone plates of a coder produces a shadow in the detector, called Moiré pattern. The spacing (S) between two adjacent fringes in the Moiré pattern is determined by the orientation of the rays, hence on the source position in the field of view and is governed by the relation (Desai et al., 1998),

$$S = \frac{r_1^2}{D \, tan\theta},$$

(8)

where r_1 is the inner zone radius, D is the spacing between two zone plates and θ is the off axis angle of the source, i.e, the angle made by the source position with the common central axis of the two zone plates. We can find the source position by measuring the fringe separation in the pattern and also the information on intensity can be obtained from the strength of the shadow.

In Figure 1(a-b), we present two Moiré fringe patterns generated by simulations for one of our FZP coder configuration (CONFIG-4: FZP2 + CMOS), one of which is for an on-axis source (Figure 1a) and the other for an off-axis source (Figure 1b). For on-axis source at infinite distance, the rays fall on the front zone plate exactly face on and two plates are exactly parallel to each other. So the rear zone plate is exactly shadowed by the front one and the fringe pattern resembles exactly a single FZP pattern (Figure 1a). But in Figure 1b, as the source is at an off-axis position by an offset of 300 arcsec, straight line fringes appear in the pattern.
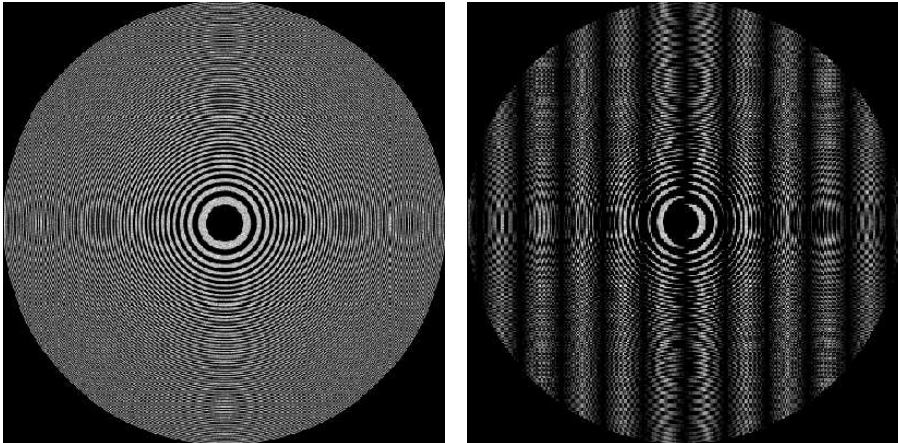

Fig. 1 Moiré patterns obtained (simulated) with a cosine negative zone plate pair for an on-axis (a) and an off-axis (b) source position.

2.2.2 Image reconstruction

As the shadow pattern is a part of Fourier transform, we can reconstruct the observed part of the sky by applying Inverse Fourier transform on the photon distribution ar-

ray obtained in the detector plane (Mertz 1965). During the image reconstruction, a computer developed FFT code is used to do the inverse Fourier transform.

As a single set of FZP coder gives a part of the Fourier transform, the inverse Fourier transform returns extra objects other than the required source (Chakrabarti et al., 2009). These include a pseudo source (ghost image) exactly at the position of mirror reflection of the actual source, and a central DC-offset. If we use two pairs of zone plates with suitable specifications, we can remove the pseudo-source. By using four suitably combined pairs of zone plates, we can also remove the central offset (Palit et al., 2009).

For a point source at finite distance, the reconstructed source looks like a dark circular spot (as can be seen in Figure 15(b) and Figure 16(b)). This spreading, which deteriorates the angular resolution of the instrument is due to the divergence of the photon beam incident on the front FZP plate (Palit et al., 2009). Diverging effect can be rectified by modifying the zone radii of the second FZP plate (Palit et al., 2009).

2.3 Configuration details

It is already mentioned that RT-2/CZT payload consists of different types of coders and detectors for imaging in hard X-rays of solar flares. In this section, we present the configuration details of the RT-2/CZT payload. The specifications of the detectors used in the payload are given in Table 1.

2.3.1 Detector specifications

Table 1

Detectors	CZT (3 numbers)	CMOS (1 number)
Dimension (cm)	4×4	2.5×2.5
Number of pixels	16×16	512×512
Pixel dimension	$(2.5 \times 2.5)\ mm^2$	$(50 \times 50)\ \mu^2$
Geometric area	$(4 \times 4)\ cm^2 \times 3$	$(2.4 \times 2.4)\ cm^2$

2.3.2 Coder specifications

We have two different types of shadow-casting devices (coders), namely, CAMs and FZPs. Two different types of CAM pattern are used for two CZT modules, whereas two pairs of zone plates with different dimensions are used for one CZT module and CMOS detector. The specifications of the coders those are used in RT-2/CZT payload are given in the Table 2.

Table 2

Device (coder)	CAM	Dual FZP
Material	Tantalum	Tungsten
Thickness(mm)	0.5	1 (each FZP)
No. of device	2	2
No. of plates in a device	1	2
Area of coder plates	16 cm^2	7.06 cm^2 for FZP1
		4.52 cm^2 for FZP2
Spacing between plates	——	32 cm for FZP1 & FZP2
Spacing between	40 cm	8 cm
coder and detector		(lower FZP to detector)
Coder shape	Square	Circular zones
No. of coder element	$16 \times 16 = 256$	151 for FZP1
		144 for FZP2
Smallest coder size/width	2.5 x 2.5 mm^2	50 μ for FZP1
		41 μ for FZP2

FZP1 is a 'positive' cosine type and FZP2 is 'negative' cosine type coder. The front view of collimator containing all the shadow-casters (coders) is shown in Figure 2.
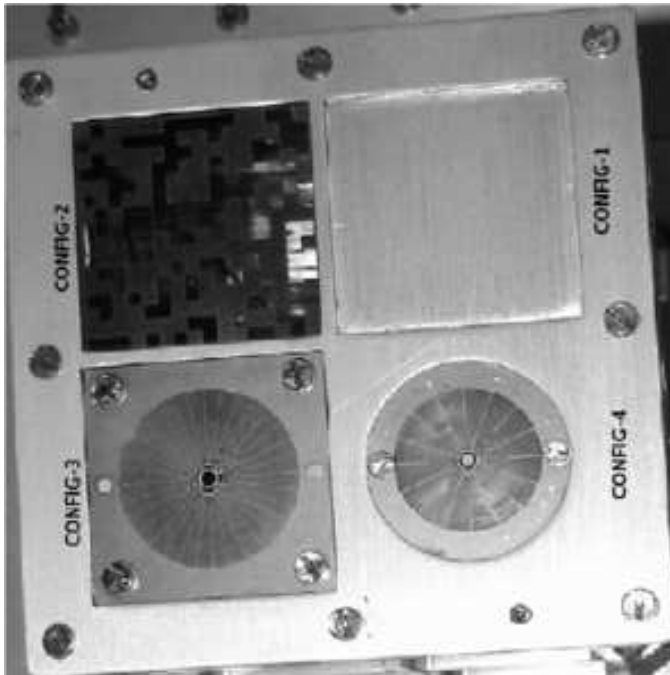

Fig. 2 Front view of the collimator displaying all the coders. One CAM is shielded with 1 mm Al sheet (CONFIG-1) and the other one is open to the sky (CONFIG-2). Front plates of FZP1 (CONFIG-3) and FZP2 (CONFIG-4) are also shown.

2.3.3 Detector-Coder combination

Detectors and coders are placed at the two ends of the collimator of the payload. The collimator is divided into four quadrants with a height of 32 *cm*. Each quadrant with coder and detector is an independent configuration and it is termed as *CONFIG*. Therefore, RT-2/CZT payload has four configurations that are summarized in the Table 3.

Table 3

Configuration	Combination	Angular resolution	FOV
CONFIG-1	CAM1 + CZT1	21.5 arc-minute	5.72 degree
CONFIG-2	CAM2 + CZT2	21.5 arc-minute	5.72 degree
CONFIG-3	FZP1 + CZT3	64 arc-sec	409 arcsec
CONFIG-4	FZP2 + CMOS	54 arc-sec	4.29 degree

3 Angular resolutions (ARs) and field of views (FOVs) of the coders

In imaging, angular resolution (AR) and FOV are the crucial aspects which determine the sensitivity and effectiveness of the instrument. Generally, angular resolution of an instrument depends on the smallest coder element size and separation between the coder and the detector. In the RT-2/CZT payload we are using various types of coders and detectors in different configurations and we present the calculation of the AR and FOV of all four configurations. The angular resolution of any coder-detector system can be calculated using the schematic diagram shown in Figure 3. Let us consider the case of CAM, where AB is the size of a single CAM element and CD is the size of a detector pixel. Now, if two sources have to be resolved by the imaging system, the rays coming from the two sources to any pixel must pass through different CAM elements. Hence the separation between the two points where the rays from the two sources (which falls on the same detector pixel) fall on two different CAM pixels must not be less than AB. The angle subtended by this minimum distance on any point of the detector pixel is θ_p.

In case of FZP coder, the scenario would be a little different. Here, AB and CD would be the radii of finest zones of the front and rear zone plates. But as every point of the finest zone is equivalent for imaging purpose, the angular resolution should be θ_r rather than θ_p (Palit et al., 2009).

To calculate the field of view (FOV), we use the same kind of picture as shown in Figure 3. But for different configurations containing CAM and CZT detector, we have to replace AB and CD by an edge of CAM and the detector respectively and for configurations containing FZPs, we have to replace them by the diameters of the zone plate (FZP1 & FZP2) far from detector and the zone plate (FZP1 & FZP2) nearer to the detector respectively. Now, the angle subtended by AB at the point O will be the FOV of the different configurations of the instrument.

For such coders, there is an inverse relationship between the angular resolution and the FOV. Since the total height of the coding device is fixed (due to satellite constraints), some maneuverability was available for the FZP in terms of the spacing between the two FZP coders. If we decrease the spacing between the two zone plates, the FOV will increase but resolution would be poor. In our instruments, we have maintained a balance between them.
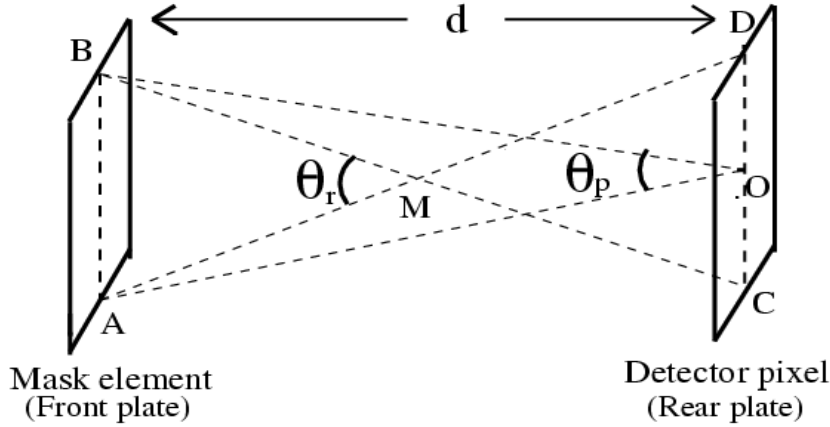
Fig. 3 Schematic diagram to compute angular resolution of CAM and FZP coder. In the figure, AB and CD are the size (width) of one single CAM element (finest zone in FZP) and detector pixel respectively.

In the RT-2/CZT payload, there are four configurations in which two different CAMs are used with two identical CZT detector modules, whereas for other two configurations dual FZPs are used with CZT and CMOS detectors respectively. The configuration details are given in Table 3.

CONFIG-1 contains CAM1 as the coder and CZT1 as detector. Smallest coder element size (AB) is of 0.25 cm and spacing between CAM1 and CZT1 is 40 cm. So the angular resolution comes out to be 21.5 $arcmin$ and FOV is 5.72°.

CONFIG-2 also contain a CAM (CAM2) and a CZT detector (CZT2). In this case, as the parameters are the same as that of previous one the angular resolution and FOV have the same value as the previous configuration (CONFIG-1).

In CONFIG-3, the coder is dual FZP (FZP1) with diameter 3.0 cm and the finest zone width is 0.0050 cm. The spacing between the two zone plates is 32 cm. The angular resolution comes out to be 64 $arcsec$. Unlike the other cases, in FZP configurations, the FOV is not determined by the diameter and spacing only. Finite size of the detector pixel actually put limitation on the FOV (Chakrabarti et al., 2009 & Palit et al., 2009). As fringe separation decreases with an increase in the off-axis angle of the source, the detector pixel can not differentiate two adjacent fringes if the separation between them goes below the detector pixel size for any large off-axis source. Hence, reconstruction of those sources is not possible. Detector pixel limited FOV for this configuration (CONFIG-3) is found to be 409 $arcsec$ wide.

CONFIG-4 is designed with dual FZP (FZP2) as shadow-caster of diameter 2.4 cm and a high spatial resolution CMOS as a detector. The width of outermost zone is 0.0041 cm and the spacing between two FZP is 32 cm. The maximum achievable angular resolution is around 54 $arcsec$ and FOV is 4.29°.

In the present configuration, the FZP coders have superior angular resolution compared to CAM. In the case of FZP with CZT detector (CONFIG-3) configuration, the FOV is limited by large pixel size of detector to a very small value. The configuration

of CMOS detector with FZP is the most viable option to image the hard X-ray solar flares.

4 Simulations

All the shadow casters along with the detectors, when placed in orbit to grab images of the source, receive parallel rays of radiation as the sources are effectively at infinite distance. In general, it is difficult during laboratory experiments to have a source which is at an infinite distance so that the shadow caster can receive parallel beam of X-rays. For experimental arrangements however large the X-ray source distance is made, the effect of divergence of the beam appears in the reconstructed source figures as can be seen in the laboratory results corresponding to the FZP coders (see §6). Though with some modifications in one of the coder plates such effects can be rectified (Palit et al., 2009), with the present configuration (employed in RT-2/CZT payload) of the zone plates effect of the divergent beams cannot be eliminated. Further, it is also difficult to have more than one hard X-ray source to study the properties of angular resolution and FOV. One of the ways to understand the characteristics of the coders and to examine their efficiency in getting images is to simulate extensively all the required cases for all four configurations keeping all the parameters and environment intact.

Simulations are done for every configuration and for all cases involving varying number of sources, with large off-axis angle of source for the verification of FOVs and for closely placed sources to verify the mathematically obtained angular resolutions. The infalling photon number on the front coders (CAM1, CAM2, FZP1 and FZP2) of all four configurations is chosen to be 5×10^5, while considering a single source. For double or multiple sources with varying intensity, photon numbers for the brightest source remains the same and photon numbers for relatively lower intensity sources are mentioned in respective sections. This number is sufficient for hundred second (on-board accumulation time for each frame) data accumulation by the imager (4 different configuration for imaging in RT-2/CZT payload) from a C class flare (and above) that occur on the surface of the Sun.

Simulation results are interpreted based on the 2D and 3D representations of the reconstructed source position and relative strength of the peaks. Source intensity variation in reconstructed image plane is plotted in arbitrary units. Detailed simulation results for all four configurations are presented in the following sections.

4.1 CONFIG-1: CAM1 + CZT1

CONFIG-1 consists of a single coder CAM (CAM1) and a CZT (CZT1) module and both are placed 40 cm apart in the first quadrant of the collimator. CAM pattern for this configuration is shown in Figure 4(a) (top left). The CAM pattern is generated from the first polynomial given in section 2.1.1. A source position is generated at a position of $\theta = 42°$ and $\phi = 1°47'$. The angle θ is measured taking positive horizontal axis as polar x coordinate ($\theta = 0°$) and ϕ is the angle from the vertical axis. The shadow of CAM due to this source on detector plane is shown in Figure 4(b) (top right). The shift of shadow pattern of the CAM from central position has coded the information on the position of source with respect to the central point in FOV. Reconstruction of the image (source position) from the CAM pattern is done according to the method

discussed in section 2.1.2. In Figure 4(c)(bottom left) and Figure 4(d) (bottom right), we have shown the 2D and 3D view of the reconstructed source (image). In both the figures of the reconstructed sky plane, the FOV is 5.72° wide along each sides. The reconstructed source position as we evaluated from Figure 4(c), matches with the actual source position assigned during simulation. From Figure 4(d), we also get a measure of the actual intensity of the source.
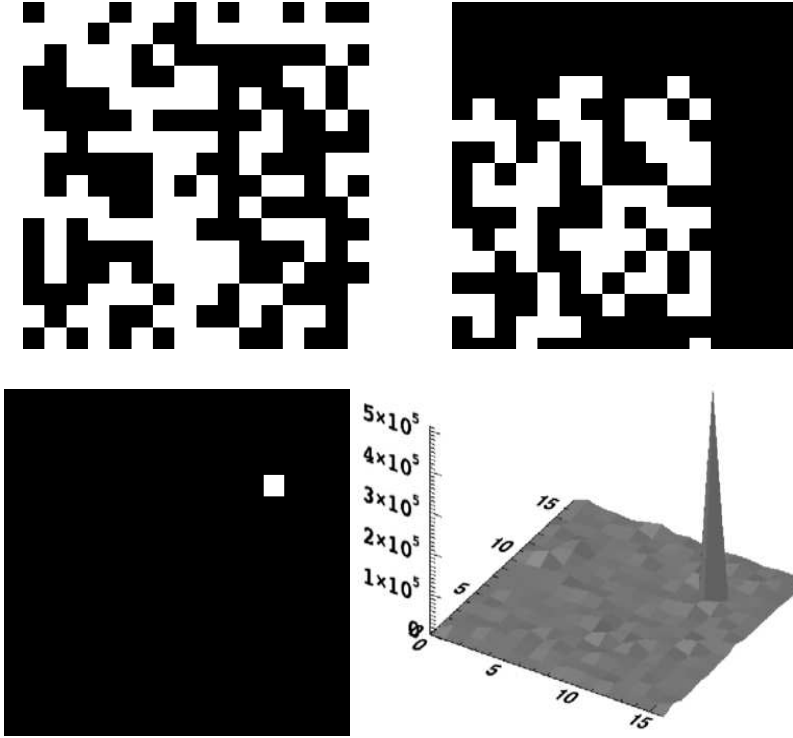

Fig. 4 (a) Simulated picture of CAM1 pattern, where opaque elements are coded by black color. (b) Shadow pattern obtained in the CZT detector for CONFIG-1 for a single source. (c) Two dimensional view of reconstructed sky plane. (d) Three dimensional picture of the source plane obtained by reconstruction.

In Figure 5(a-c), we present the simulation results to verify the accuracy of the mathematically obtained angular resolution of the configuration containing CAM1 and CZT1. For this, we have placed two sources at an angular separation of 21.5 arc-minute from each other. The number of photons falling on the CAM from the brighter source is 5×10^5 and that from the fainter one is 2.5×10^5. In Figure 5(a), we have shown the shadow pattern obtained for two sources which are placed very close to each other. The reconstructed source (image) in 2D and 3D view of both the sources are shown in Figure 5(b)(top right) and 5(c)(bottom). It can be seen from the figures that the two sources are separated by one pixel between them. So the sources can be said to be just resolved.
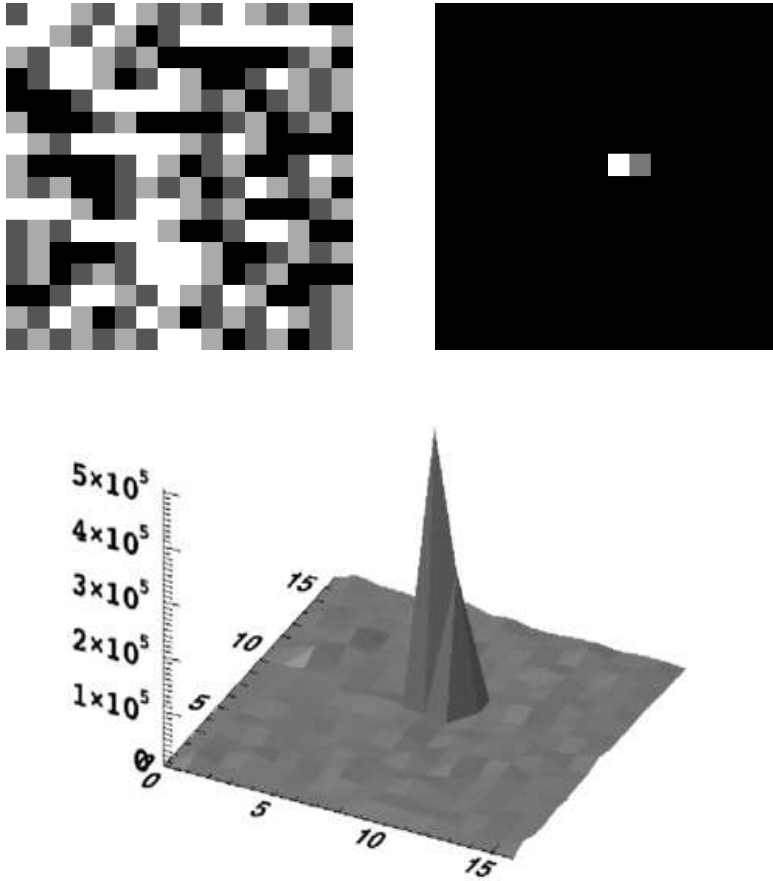
Fig. 5 (a) Shadow pattern obtained for two sources placed very close to each other (21.5 arc-min) with CAM1 and CZT1 (top left) configuration. (b) 2D view of reconstructed sky plane (top right). (c) 3D view of the source intensities obtained by reconstruction (bottom).

The CONFIG-1 and CONFIG-2 are identical as both configurations use CAM and CZT except the CAM patterns are different in CAM1 and CAM2. Therefore, the FOV and angular resolution in both configuration are mathematically the same.

4.2 CONFIG-2: CAM2 + CZT2

The CAM used in this configuration is different from the CAM pattern of CONFIG-1. The CAM2 pattern is generated from the second polynomial given in section 2.1.1 and is shown in Figure 6a (top left). Simulation results for CONFIG-2 (CAM2 and CZT2) are shown in Figure 6(b,c,d). In this case, we have considered two sources in the field of view of the collimator with position $\theta = 227° \, 30'$, $\phi = 3° \, 00'$ and $\theta = 90° \, 00'$, $\phi = 00°$ $32'$ respectively. Number of X-ray photons falling on CAM2 from the two sources are the same (5×10^5 counts). In Figure 6b (top right), we have presented the combined shadow pattern of the CAM (CAM2) generated by the two sources.
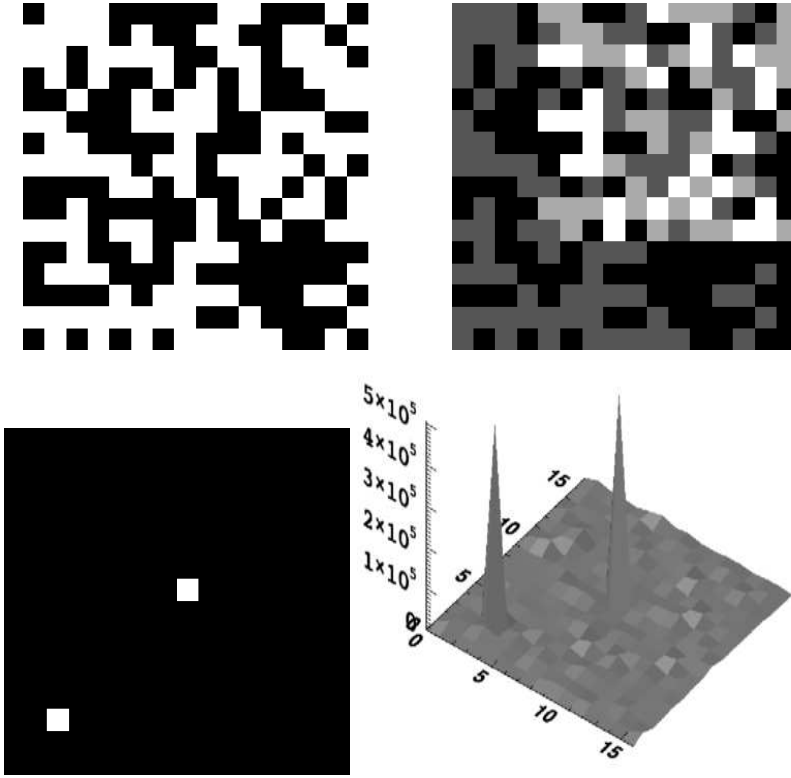
Fig. 6 Simulated picture (opaque elements of the pattern are coded by black color) of CAM used in CONFIG-2 (top left). (b) Shadow pattern obtained for two sources (top right). (c) 2D view of reconstructed sky plane (bottom left). (d) 3D picture of the sources obtained by reconstruction (bottom right). See text for details.

The shifts of individual shadows produced by each source is compatible with their positions as can be seen from the Figure 6. In Figure 6c (bottom left), we have presented the 2D picture of the reconstructed object plane. From this figure, we get the exact information about the positions of the two sources. These positions agree with the assigned positions of the sources during simulation. From Figure 6d (bottom right), which is the 3D view of the reconstructed source plane, we get the information on the relative brightnesses of the sources. The two peaks correspond to the two reconstructed sources and they are found to be of the same height (intensity). It is clearly seen from this simulation that the relative brightnesses of the sources in reconstructed plane are exactly replicated irrespective of their relative positions whereas in case of many other imaging devices there may be position dependencies of relative intensities of the reconstructed sources.

In the next simulation step, we place two sources at extreme right and left ends of the collimator wall to verify mathematically calculated FOV. Sources are placed at $\theta = 0°$ and $\theta = 180°$ with common ϕ angle of value $2.86°$. It is clearly seen from the reconstructed images that the sources are really placed at the two extreme edges of the collimator and their separation is the measured value of FOV. In Figure 7(b, c), 2D and 3D view of the reconstructed images of the sky plane with two sources are shown.
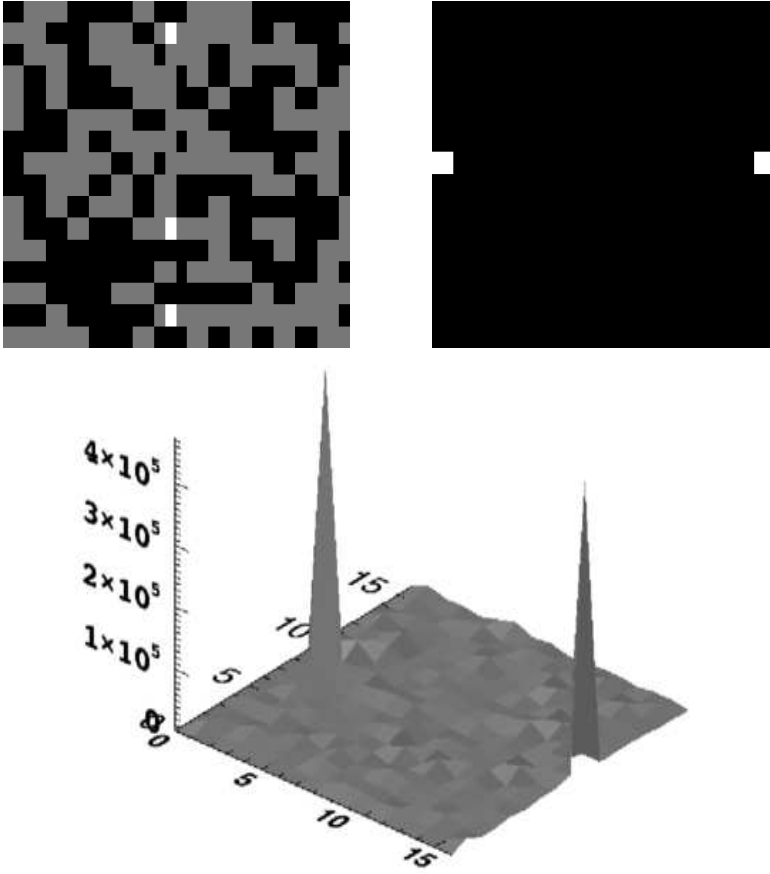
Fig. 7 (a) Shadow pattern of CAM2 for two sources placed at two extreme ends of FOV (top left), (b) 2D view of reconstructed sky plane (top right).(d) 3D view of the sources obtained by reconstruction.

4.3 CONFIG-3: FZP1 + CZT3

The CONFIG-3 consists of a pair of Fresnel zone plates (FZP1) as a coder and a CZT module (CZT3) as detector. Both the FZPs have inner radii of 0.122 cm and the number of zones in each is 151. The pair is a positive cosine one, i.e, the nth zone radius for each of the zone plates is equal to $\sqrt{n}$ times the inner radius and the central zones are transparent to X-rays. CZT detector consists of 256 pixels having dimension of 0.25 cm $\times$ 0.25 cm.

In Figures 8(a-c), we have plotted the fringe and reconstructed sources for a single source placed at $\theta = 116°$ and $\phi = 170''$. We have chopped out the central DC-offset (Chakrabarti et al. 2009) to get the prominent source picture, while plotting the reconstructed images. A pseudo source apart from the original source position is seen in the reconstructed image. Combination of cosine and sine FZPs can remove the effect of ghost image (pseudo source). The finite size of the detector pixel restricts the field of view to $409''$.
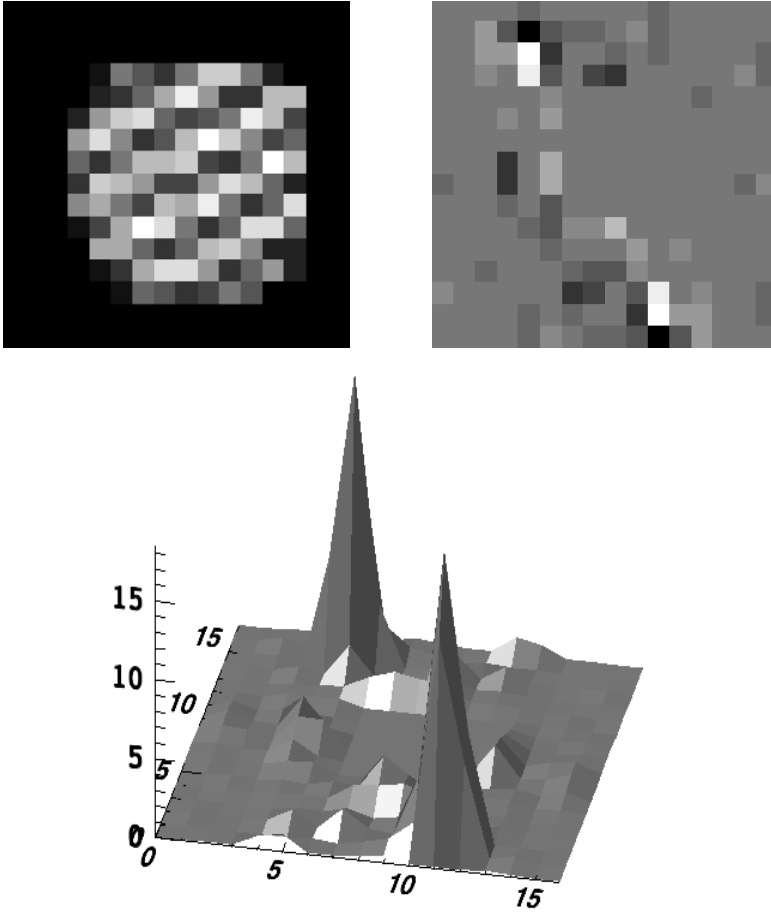
Fig. 8 (a) Fringes obtained on CZT3 detector with FZP1 as coder (top left). Two sources appear in the reconstructed 2D (b) and 3D (c) image plane, one of which is the pseudo source of the actual source. The central DC-offset is chopped out.

FOV calculated for this configuration can be verified from the simulation too. For the simulation, we have considered a single source placed at $\theta = 0°$ and $\phi = 204''$.

In Figure 9(a-c), we have plotted the fringe pattern along with 2D and 3D reconstructed source in the detector plane. It is seen that the reconstructed source (also the pseudo source) is at extreme edge of the reconstructed array. This confirms that the FOV of the instrument is actually twice the angle of ϕ, i.e, $409''$.

We have also carried out simulation to verify the angular resolution achievable by this configuration. According to the design specifications, the calculated angular resolution is around $64''$ (see section 3). In Figures 10(a-c), we have presented the combined fringes and reconstructed 2D and 3D views of reconstructed sky plane of two closely placed sources. The sources are placed at roughly 64 arc-sec apart. From the 2D (top right) and 3D (bottom) images of the reconstructed sources, we find that two sources are just resolved. Hence we can conclude that the mathematically found angular resolution is well supported by simulations.
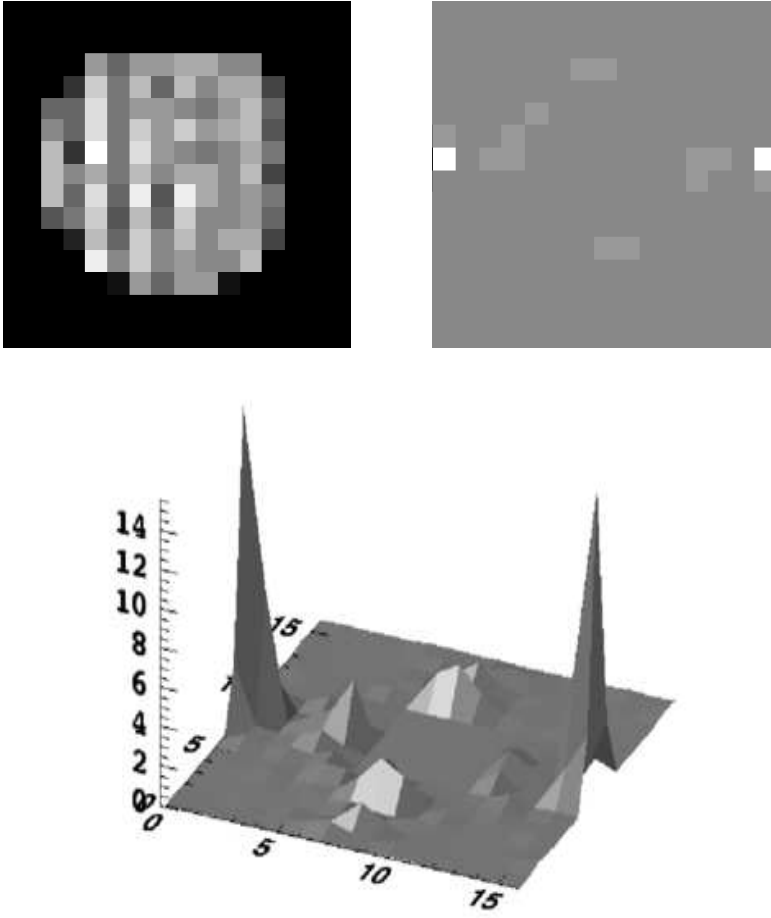
Fig. 9 (a) Fringes obtained on a CZT detector combined with a FZP coder (top left). The source is at extreme right edge of the reconstructed sky array shown in the reconstructed 2D (top right) and 3D (bottom) view.

4.4 CONFIG-4: FZP2 + CMOS

CONFIG-4 is the best possible configuration for imaging of a hard X-ray source in terms of achievable angular resolution. This configuration consists of dual FZP (FZP2) coder with a finest zone width of 0.0041 cm and high position sensitive CMOS detector with smallest pixel size of 0.005 cm. The FZP coder is of negative cosine type. Inner zone radius of each zone is 0.1 cm and number of zones is 144.

The simulated Moiré fringe pattern for on and off-axis source position is shown in Figure 1. Now, we simulate for FOV verification of this configuration. We have considered a single source with offset angle $\phi = 2.145^{\circ}$ and $\theta = 0^{\circ}$.

The Moiré fringe pattern for the source with offset $\phi = 2.145^{\circ}$ is shown in Figure 11(a). In Figure 11(b), 3D view of the reconstructed source plane is shown along with
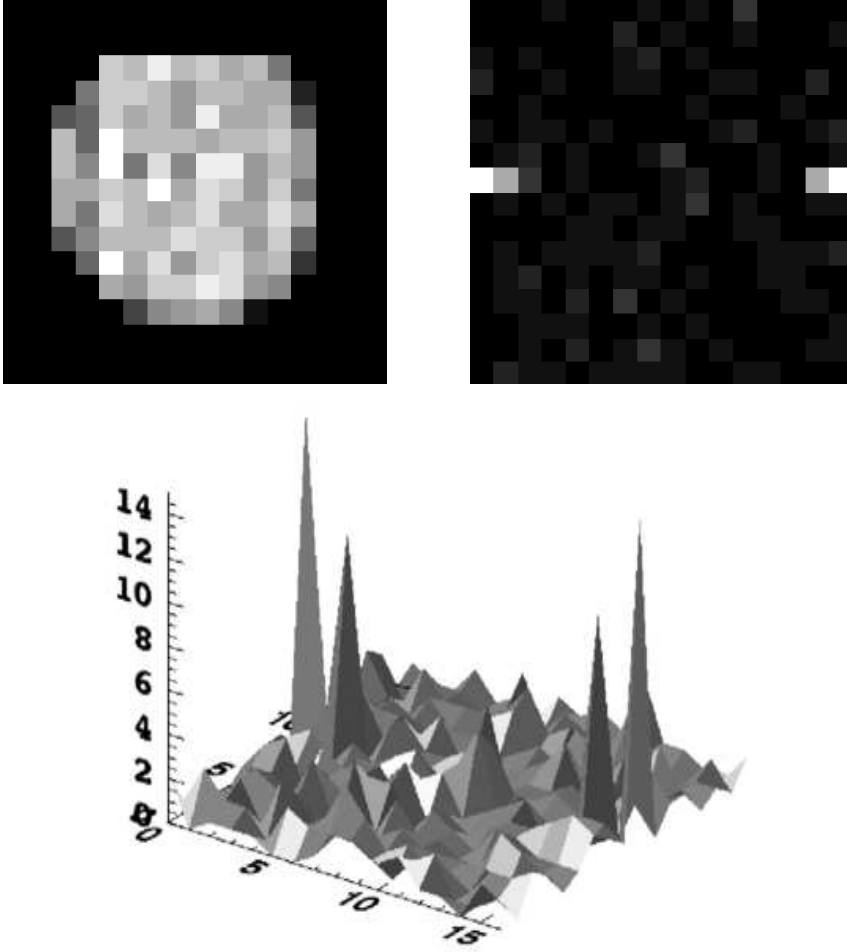
Fig. 10 (a) Fringes for two closely placed sources in the limited FOV of CONFIG-3 (top left). (b) Sources appear to be very close and just resolved in the reconstructed 2D (top right) and 3D (bottom) images. Sources at right side of central point in reconstructed plane represent the actual sources. Pseudo source (ghost image) is also seen in the reconstructed image plane along with the background noise.

the pseudo source (ghost source). Reconstructed source plane shows that the source is at extreme end of the FOV of the collimator, which confirms that the FOV is actually $4.29°$ (twice the ϕ value).

The most important aspect of this configuration is the best possible angular resolution which could be around $54''$. To verify the mathematically calculated angular resolution value, we simulate with two sources placed $54''$ apart and less than that. From simulation, it is found that the sources which are placed less than $54''$ apart are not resolvable at all. In Figure 12(a,b), we have shown the fringe pattern and reconstructed sky plane of two sources which are separated by $54''$. The double pseudo
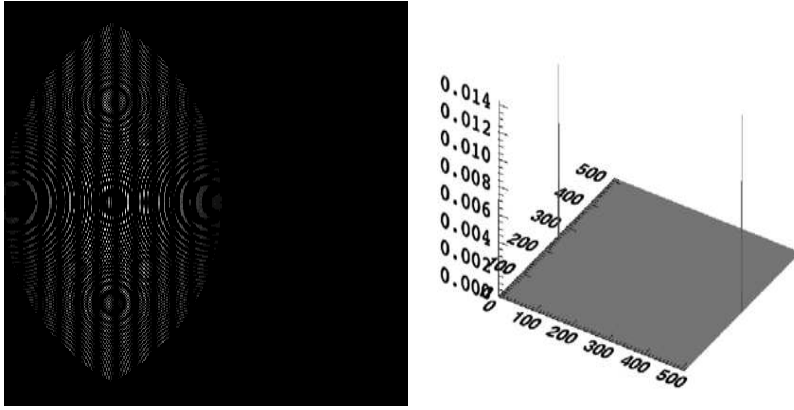
Fig. 11 (a) Fringes obtained on a CMOS detector with a pair of zone plates as coded aperture (left). (b) 3D picture of the reconstructed source along with pseudo source which also appears in the reconstructed source plane. The central DC offset is chopped out.
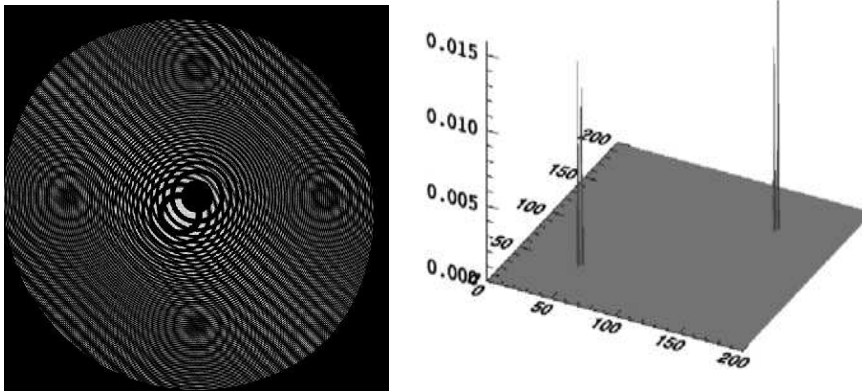

Fig. 12 (a) Fringes obtained (left) with a pair of sources at angular distance from each other equal to the calculated angular resolution ($54''$) of the FZP2-CMOS combination. (b) 3D view of the reconstructed sources. To get a closer view, the part of the reconstructed plane containing the sources is zoomed, so that out of 600 hundred pixels along each side only 200 pixels are shown.

source (ghost image) is also seen in the 3D view. Separation between the two closely placed sources are found to be equal to one detector pixel dimension.

So far, we have considered a point source to do the simulation. In principle, it is also possible to do simulation for extended sources. Simulation is done for the same configuration (CONFIG-4) with large number of point sources, which can be conveniently taken as an extended source. The fringe pattern along with 2D and 3D views of reconstructed sources are given in Figures 13(a-c). Amplitudes of individual reconstructed source give their relative intensities in the extended source distribution.
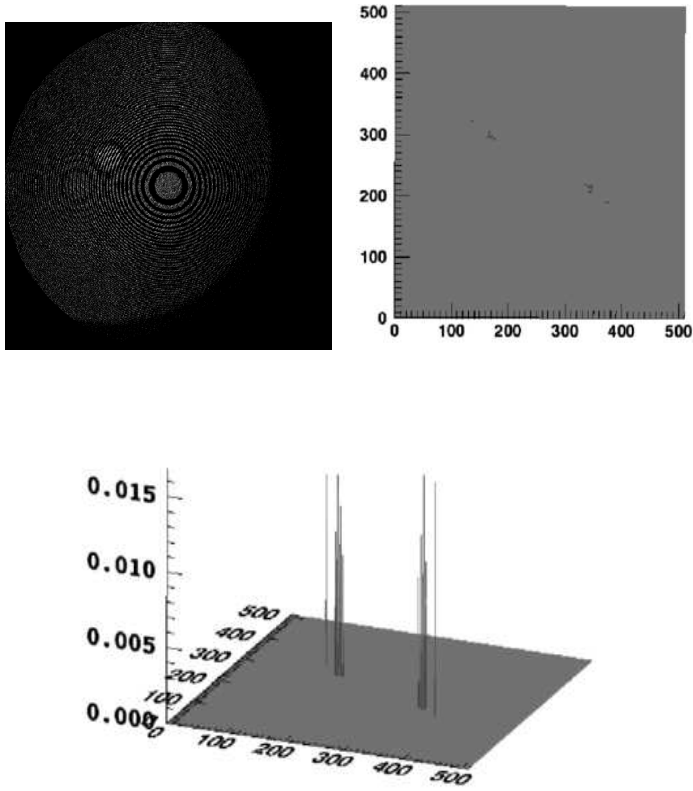
Fig. 13 (a) Fringes obtained with a pairs of zone plates on CMOS detector for multiple sources (extended source) (top left). (b) 2D view of the reconstructed sources (top right). (c) 3D view of reconstructed sources of the sky plane.

5 Expectations in the context of solar observations

The prime objective of RT-2 Experiment onboard CORONAS-PHOTON satellite is to study the solar hard X-ray emission associated with solar flares. Solar flares are the most powerful explosions on the Sun, when the stored energy in twisted magnetic field is suddenly released. Solar flares are generally classified according to their X-ray brightness in the wavelength range of 1 to 8 Å. Intensity of the classified flares (eg. A, B, C, M and X class) are measured based on the peak flux (in unit of W/m^2) which is measured on the GOES satellite. X-class flares are the most intense having peak flux of 10^{-4} W/m^2, while A-class flares are weakest of having peak flux of 10^{-8} W/m^2. The peak flux of each class is 10 times greater than the preceding one with a linear division of 9 within each class. Therefore, a C4.0 class flare is 11 times more powerful than a B3.0 class flare.

The spectral and temporal characteristics of solar hard X-ray flare are diverse, ranging from relatively soft, thermal (kT ≈ 10 keV) spectra, to hard, power law spectra, and from strong micro-flares with duration of seconds to events lasting 30 minutes or more. Therefore, the evolution of hard X-ray emission regions with time is an important

aspect for better understanding of physics involved in the emission process. To pin-point the emission regions, it is essential to have high angular resolution instruments. The RT-2/CZT payload which is designed with four different configurations (in terms of AR and FOV) will serve the main purpose to image the solar flares with high angular resolution.

Normally, the Sun is quiet to the level of being invisible in the hard X-ray and γ-ray energy band. The hard X-ray and γ-ray detection of Sun is necessarily a study of energetic solar flares of flare strength not less than B3.0.

We have considered that the maximum number of photons hitting the coder surface is around 5×10^5 (at least for one source), while performing the simulations for all four configurations. In a realistic situation, like a solar flare of X4.8 type, which occurred on 2002 July 23, (during the previous solar cycle), we have estimated the response of the particular flare for all four configurations. The spectrum of the giant flare during impulsive phase is double power-law like nature (Lin et al. 2003) with indices $\gamma_L \approx 6.2$ below and $\gamma_H \approx 2.8$ above a sharp break around 30 keV with a maximum flux around $5 \times 10^3 photons/sec/cm^2/keV$ at 20 keV. Using the above spectral information, we have calculated the number of photons impinging on each coders (four configurations) for 100 sec accumulation (onboard accumulation time of each image frame) at different energy bands. Apart from the real observation, we have also calculated the number of photons impinging on each coder surface for a typical flare of C3.5 type, which is characterized by a spectrum of single power law of index $\gamma \approx 4.0$ and flux (maximum) around 200 $photons/sec/cm^2/keV$ at 20 keV. The estimated photon counts which impinges on all four configurations for both the flares, are given in the Table 4.

Table 4

Class	Energy	CONFIG-1	CONFIG-2	CONFIG-3	CONFIG-4
	(keV)	Counts	Counts	Counts	Counts
	(20-50)	1.22×10^7	1.22×10^7	5.38×10^6	—
X4.8	(50-100)	2.12×10^6	2.12×10^6	7.31×10^5	—
	(20-100)	1.43×10^7	1.43×10^7	6.31×10^6	4.04×10^6
	(20-50)	6.24×10^5	6.24×10^5	2.75×10^5	—
C3.5	(50-100)	3.70×10^4	3.70×10^4	1.62×10^4	—
	(20-100)	6.61×10^5	6.61×10^5	2.91×10^5	1.88×10^5

It is evident from the estimations given in Table 4, that we could detect clear and prominent fringes for flares like X4.8 and as low as C3.5 type flare with all four configurations. For less intense flares as low as B type flares, though there may not be images with prominent fringes in the detectors but after proper reconstruction it could still be possible to reproduce the sources in the field of view.

The FOV (5.72°) of CAM and CZT detector (CONFIG-1 and CONFIG-2) is enough to accommodate the whole Sun. Due to poor angular resolution ($21.5'$), it is hardly possible to observe and distinguish more than one flare, simultaneously. Imaging of a single flare with CONFIG-3 is more critical as the FOV in this configuration is very small ($409''$). Therefore, a highly pointed observation (within $409''$) of flare with this configuration is possible to image with moderate angular resolution ($64''$). On the other hand, the imaging of full Sun with hard X-ray solar flares is nicely possible with the CONFIG-4, as the FOV (4.57°) and angular resolution ($54''$) are superior compared to any other configuration.

6 Laboratory test results

Tests with CONFIG-2 (CONFIG-1) set up were carried out at laboratory of VSSC, Thiruvananthapuram, India. The set up consists of single plane coder (CAM2) and CZT (CZT2) detector. The CAM is shined with a strong radio-active source placed on top of the collimator at position of $\theta=150^\circ$ (approx) and $\phi=1.04^\circ$. In Figure 14a (top left), the shadow pattern of the CAM obtained in the CZT detector is shown. In Figures 14b (top right) and 14(c, d) (bottom-left: source with background noise, bottom-right: background noise is averaged out), we have shown the 2D and 3D view of the reconstructed source plane. The source in the reconstructed plane (detector plane) is nearly exact reproduction (in terms of position and intensity) of the original source. The source, though actually a point source, is spread over two pixels of the reconstructed image plane. It is due to the divergent nature of rays from the radio-active source, which impinges on the coder (CAM2), placed at 132 cm away from the detector plane.
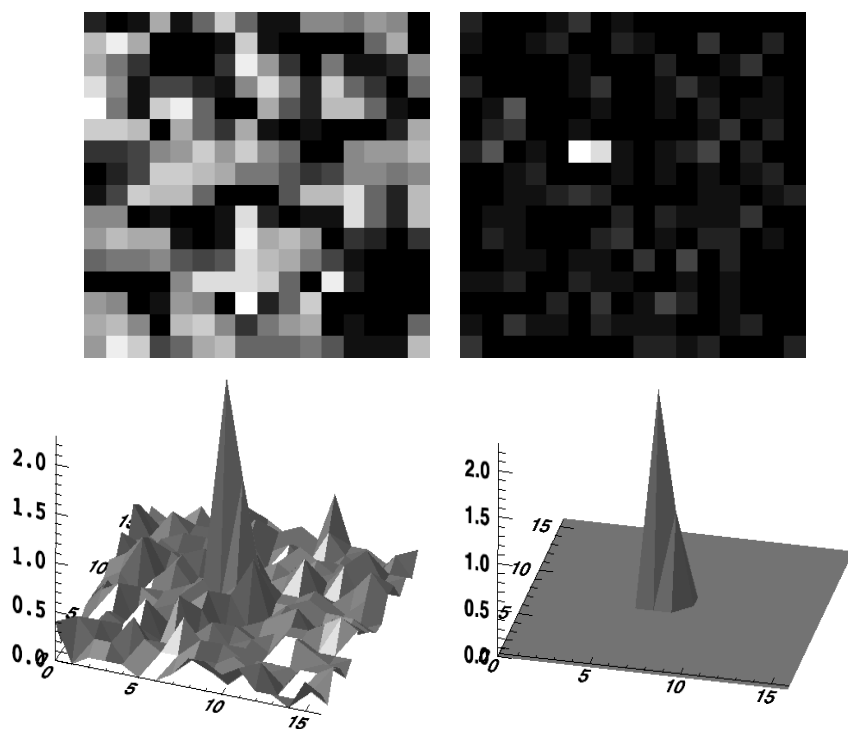

Fig. 14 (a) Shadow pattern obtained during tests with a CAM on a CZT detector for a single source (top-left). (b) 2D picture of the reconstructed source (top-right). (c) 3D picture of reconstructed source with background noise. (d) 3D view of the reconstructed source after smoothing the background noise.

Tests with FZP set up were carried out at the X-ray laboratory of ICSP, Kolkata, India which is equipped with an X-ray source generator of operating voltage 5 Volt to 50 Volt. As it is difficult to produce parallel X-ray beam at laboratory, we have

generated quasi-parallel (diverging) X-ray beam with 45 feet collimator made of lead shielded aluminum pipe. The detector system (collimator having FZPs and detector) is kept at one end of the 45 feet long pipe opposite to the X-ray source.

In the first set of experiment, we have taken dual zone plates of negative in nature and the n-th zone radius for each is $\sqrt{n}$ times the inner zone radius. The inner zone radius is 0.1 cm and number of zones in each zone plate is 144 with finest zone width of 0.0041 cm. The separation between the zone plates is 32 cm. Highly position sensitive CMOS detector is used with smallest pixels size of 0.005 cm.
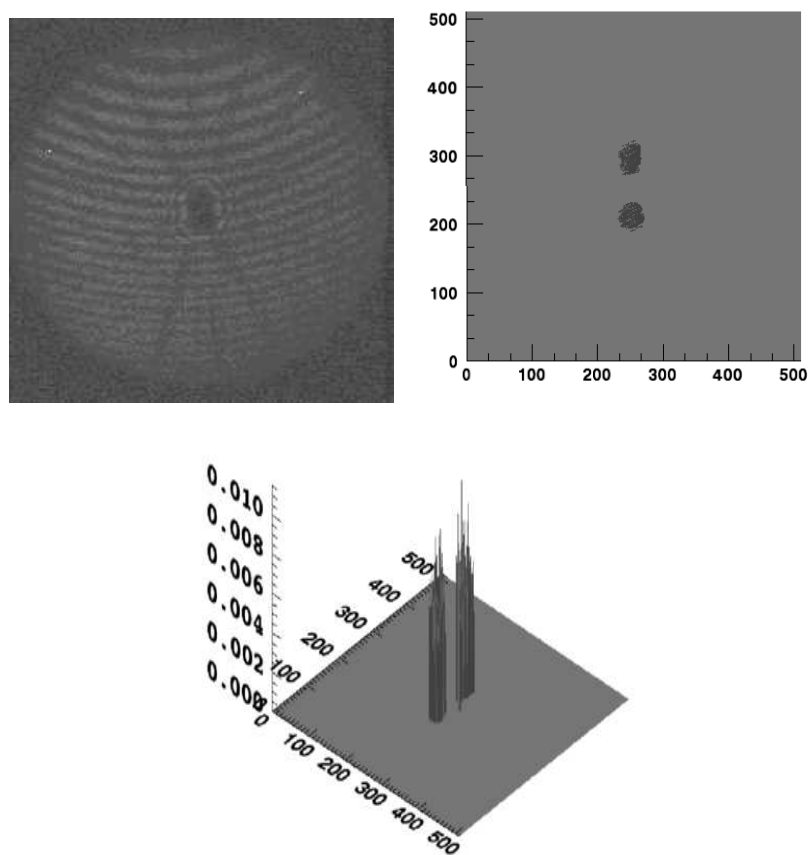

Fig. 15 (a) Fringes obtained with a pair of negative cosine FZP on CMOS detector for a slightly off-axis source (top left). (b) 2D view of the reconstructed source (top right) and (c) 3D view of reconstructed source are seen in image plane along with pseudo source (bottom).

The X-ray source is positioned at a little off-axis with the central line of beam. The Moiré fringe pattern observed in the detector plane (CMOS) is shown in Figure 15(a). In Figure 15(b,c), we have plotted the 2D and 3D view of the reconstructed point source in the detector plane. The pseudo source (ghost image) and central DC offset both appear in the experimental results. As the central DC-offset is incomparably

bigger than the reconstructed source and its pseudo part, we have to chop it out to get the source prominently. Measurement gives the off-axis angle of the source (ϕ) as $32'$ $20''$ and θ as $93°$. This is consistent with the priorly specified actual source position. The divergence of the projected X-ray photon beam has caused broadening of reconstructed source and makes it look like a circular spot.

In another experimental set up, different coder (FZP1) along with CMOS detector is used. The coder is cosine type and positive in nature. The inner zone radius of each of the zone plate is 0.122 cm and number of zones is 151 with finest zone width 0.0050 cm. The observed Moiré fringe pattern on the detector plane is shown in Figure 16(a). The reconstructed 2D and 3D images in detector plane is shown in Figure 16(b,c). Actual source (right side) along with the pseudo source (ghost image) is seen in the image. The source is offset by an amount ϕ=$21'$ $30''$ and at θ=$50°$ $31'$. The reconstructed 2D (top right) and 3D pictures (bottom left) represent exact replica of the source plane.
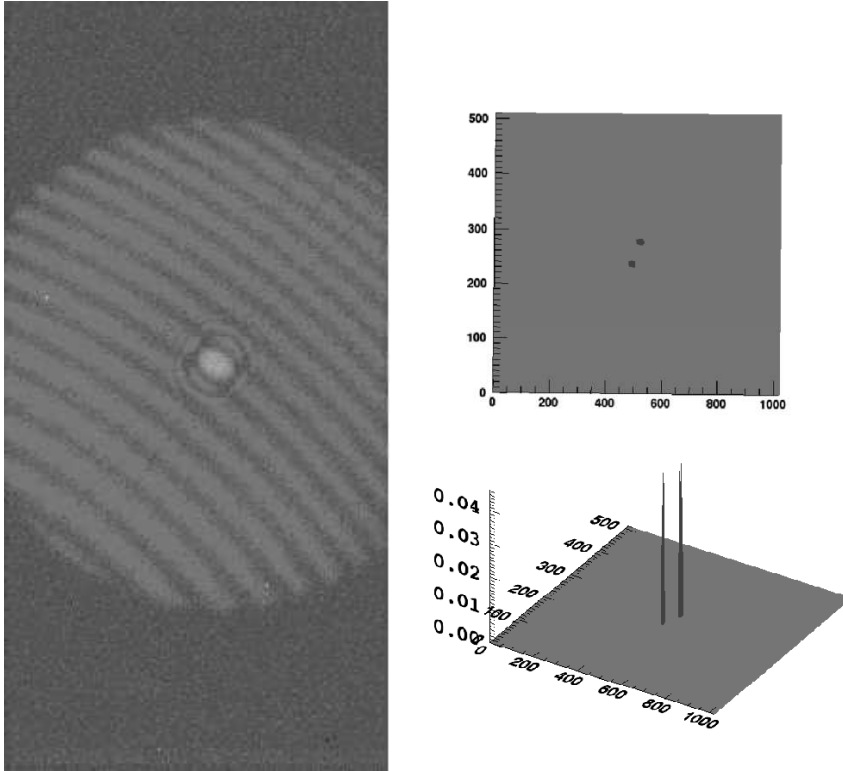

Fig. 16 (a) Fringe obtained experimentally with a pair of zone plates (FZP1) on CMOS detector for a source (top left) at offset $21'$ $30''$. (b) 2D view of the reconstructed source (top right) and (c) 3D view of reconstructed source are seen along with pseudo source.

7 Conclusion

The RT-2/CZT payload onboard CORONAS-PHOTON mission is a unique instrument for imaging in hard X-rays. It uses four different kinds of configurations with which various combinations of angular resolutions (AR) and FOVs are achievable for imaging a single source at a time. This instrument also uses FZP coder as a shadow casting device for imaging in hard X-rays in space flight, for the first time. Two different types of coders (CAM and FZP) along with two different types of detectors (CZT and CMOS) are used to achieve variable angular resolutions. As far as imaging is concerned, this mission is first of its kind as it makes use of CAM and FZP coder together as shadow caster for the first time in space based imaging.

The FZP coders, used in the CONFIG-4 along with high position sensitive CMOS detector (50 μ), have angular resolution which is much better than those of the configurations consisting CAMs and CZTs. The best geometric resolution of this instrument is around $54''$. The hard X-ray imaging devices rely on the number of photons detected, and hence the centroiding accuracy for point sources can be much better than this, and can reach upto a few arc-seconds for very bright sources. For example, the RHESSI satellite uses another alternative approach to image in hard X-rays with Rotation Modulation Collimator (RMC) technique and, depending on the source intensity, source localization accuracy ranged from $2''$ to $180''$.

It is also possible to achieve good spatial resolution with CAM-CMOS configuration. For that one has to design the CAM elements size comparable to those of CMOS pixels to maintain the consistency of spatial resolution with that of the detector. This is a much more complex effort in terms of fabrication and alignment.

In this paper, we have presented simulation results along with direct reconstruction of images to quantify the AR and FOV of the various configurations used in the payload. Some of the simulation results are verified with laboratory measurements. Since all the 4 detectors would be simultaneously imaging the same event (viz., solar flares), it should be possible to make a simultaneous fit to all the four images with a few assumed source positions and hence to accurately measure the source positions and intensity. This will mitigate some of the problems in the direct reconstruction like ghost images in the FZP images and noise patterns in the CAM images.

On 30th January, 2009, the CORONAS-PHOTON was launched successfully and all the RT-2 instruments are working to our satisfaction. However, so far, in the 24th cycle, the solar activity has been weak and we are awaiting stronger flares for direct imaging. The on-board data quality and results would be discussed elsewhere.

References

1. Ables, J. G.: Fourier transform photography: a new method for X-ray astronomy. Proc. Astron. Soc. Australia 1, 172 (1968)
2. Ajello, M., Greiner, J., Kanbach, G., Rau, A., Strong, A. W., Kennea, J. A.: BAT X-Ray Survey. I. Methodology and X-Ray Identification, ApJ, 678, 102 (2008)
3. Barrett, H. H., Myers, K. J.: Foundations of Image Science. John-Wiley, New York (2004)

4. Baker, R. E., Barbareschi, L., Bazzano, A., Butler, R. C., Caroli, E., Carter, J. N., Catani, O., Charalambous, P., Court, A. J., Di Cocco, G., Igiuni, A., La Padula, C., Morelli, E., Polcaro, F., Ramsden, D., Rubini, A., Santini, M., Spada, G., Traci, A., Ubertini, P., and Villa, G.: Adv. Space Res. 3, 95 (1983)

5. Caroli, E., Stephen, J.B., Di Cocco, G., Natalucci, L., Spizzichino, A.: SSR, 45, 349 (1987)

6. Chakrabarti, S. K., Palit, S., Debnath, D., Nandi, A., Yadav, V., Sarkar, R.: Fresnel zone plate telescope for X-ray imaging I: experiments with a quasi-parallel beam, Exp. Astron, 24, 109 (2009)

7. Debnath, D., Nandi, A., Rao, A. R., Malkar, J. P., Hingar, M. K., Kotoch, T. B., Sreekumar, S., Madhav, V. P., Chakrabarti, S. K.: Instruments of RT-2 Experiment onboard CORONAS-PHOTON and their test and evaluation I: RT-2/S and RT-2/G Payloads, Exp. Astron. (2010, in press).

8. Desai, U., Orwig, L. E., Piquet, L., Gaither, C. C.: X-ray telescope for small satellites, Proc. SPIE Vol. 3442, p.94, Missions to the Sun II, Ed. C.M. Korendyke (1998)

9. Dicke, R. H.: Scatter hole cameras for X-ray and gamma-rays. ApJ, 153, L101 (1968)

10. Fenimore, E. E., Cannon, T. M.: APO, 17, 337 (1978)

11. Gunson, J., Polychronopulos, B.: MNRAS, 177, 485 (1976)

12. In 't Zand, J. J. M.: Ph.D. Thesis, University of Utrecht (1992)

13. Kotoch, T. B., Nandi, A., Debnath, D., Malkar, J. P., Rao, A. R., Hingar, M. K., Madhav, V. P., Sreekumar, S., Chakrabarti, S. K.: Instruments of RT-2 Experiment onboard CORONAS-PHOTON and their test and evaluation II: RT-2/CZT Payload, Exp. Astron. (2010, in press).

14. Kotov, Yu., Kochemasov, A., Kuzin, S., Kuznetsov, V., Sylwester, J., Yurov, V.,: Set of instruments for solar EUV and soft X-ray monitoring onboard satellite Coronas-Photon. In 37th COSPAR Scientific Assembly, in Montral, Canada., p.1596 (2008)

15. Lin, R. P., Krucker, S., Hurford, G. J., Smith, D. M., Hudson, H. S., Holman, G. D., Schwartz, R. A., Dennis, B. R., Share, G. H., Murphy, R. J., Emslie, A. G., Johns-Krull, C., Vilmer, N.: Rhessi observations of particle acceleration and energy release in an intense solar Gamma-ray line flare, ApJ, 595, L69 (2003)

16. Mertz, L.: Transformation in Optics. Wiley, New York (1965)

17. Mertz, L., Young, N. O.: Fresnel transformation of images. In Proc. Int. Conf. on Opt. Instrum. Techniques, ed. Habell, K. J. 305, (Chapman and Hall, London) (1961)

18. Nandi, A., Rao, A. R., Chakrabarti, S. K. et. al.: Indian Payloads (RT-2 Experiment) onboard CORONAS-PHOTON Mission. In Proc. of International Conference on Space Technology, Greece, G. Lampropoulos and M. Petrou (Eds.) (2009) (arXiv:0912.4126)

19. Palit, S., Chakrabarti, S. K., Debnath, D., Rao, A. R., Nandi, A., Yadav, V. K., Girish, V.: Fresnel Zone Plate Telescopes for X-ray Imaging II: Numerical simulations with parallel and diverging beams, Exp. Astron, 27, 77 (2009)

20. Peterson, W. W.: Error Correcting Codes, (Massachusetts: MIT Press) (1961)

21. Sarkar, R., Mandal, S., Debnath, D., Kotoch, T. B., Nandi, A., Rao, A. R., Chakrabarti, S. K.: Instruments of RT-2 Experiment onboard CORONAS-PHOTON and their test and evaluation IV: Background Simulations using GEANT-4 Toolkit, Exp. Astron. (2010, in press).

22. Sreekumar, S., Vinod, P., Samuel, E., Malkar, J. P., Rao, A. R., Hingar, M. K., Madhav, V.P., Debnath, D., Kotoch, T. B., Nandi, A., Begum, S. S., Chakrabarti, S. K.: Instruments of RT-2 Experiment onboard CORONAS-PHOTON and their test and evaluation V: Onboard software, Data Structure, Telemetry and Telecommand, Exp. Astron. (2010, in press).